Bioactive Materials 6 (2021) 1541–1554

Contents lists available at ScienceDirect

Bioactive Materials

journal homepage: www.sciencedirect.com/journal/bioactive-materials

Nitrogen-doped fluorescence carbon dots as multi-mechanism detection for iodide and curcumin in biological and food samples

Xiaodan Tang [a], Hongmei Yu [a,*], Brian Bui [b], Lingyun Wang [b,c], Christina Xing [b], Shaoyan Wang [a], Mingli Chen [d], Zhizhi Hu [a,**], Wei Chen [b,***]

[a] School of Chemical Engineering, University of Science and Technology Liaoning, Liaoning, Anshan, 114051, China
[b] Department of Physics, The University of Texas at Arlington, Arlington, TX, 76019-0059, USA
[c] School of Chemistry and Chemical Engineering, South China University of Technology, Guangzhou, 510641, China
[d] Research Center for Analytical Sciences, Department of Chemistry, College of Sciences, Northeastern University, Box332, Shenyang, 110819, China

ARTICLE INFO

Keywords:
Nitrogen-doped carbon dots
Iodine ion
Curcumin
Internal filtration effect
Solid-phase thermal method
Disease
Detection

ABSTRACT

Iodine ion is one of the most indispensable anions in living organisms, particularly being an important substance for the synthesis of thyroid hormones. Curcumin is a yellow-orange polyphenol compound derived from the rhizome of *Curcuma longa L.*, which has been commonly used as a spice and natural coloring agent, food additives, cosmetics as well as Chinese medicine. However, excess curcumin may cause DNA inactivation, lead to a decrease in intracellular ATP levels, and trigger the tissue necrosis. Therefore, quantitative detection of iodine and curcumin is of great significance in the fields of food and life sciences. Herein, we develop nitrogen-doped fluorescent carbon dots (NCDs) as a multi-mechanism detection for iodide and curcumin in actual complex biological and food samples, which was prepared by a one-step solid-phase synthesis using tartaric acid and urea as precursors without adding any other reagents. An assembled NCDs-Hg^{2+} fluorescence-enhanced sensor for the quantitative detection of I^- was established based on a fluorescence "turn-off-on" mechanism in a linear range of 0.3–15 μM with a detection limit of 69.4 nM and successfully quantified trace amounts of I^- in water samples and urine sample. Meanwhile, the as-synthesized NCDs also can be used as a fluorescent quenched sensor for curcumin detection based on the synergistic internal filtration effect (IFE) and static quenching, achieving a good linear range of 0.1–20 μM with a satisfactory detection limit of 29.8 nM. These results indicate that carbon dots are potential sensing materials for iodine and curcumin detection for the good of our health.

1. Introduction

The iodine ion is one of the most indispensable anions in living organisms, particularly being an important substance for the synthesis of thyroid hormones. Iodine deficiency or excess may lead to a series of thyroid diseases, such as goiter, cretinism, hypothyroidism, autoimmune thyroid diseases and even increasing the incidence of thyroid cancer [1,2]. Iodine is an exogenous element that can not be synthesized by the human body, thus it mainly comes from drinking water or various food [3]. To prevent iodine deficiency or excessive intake, the World Health Organization (WHO) recommends daily dietary iodine intake of 150 μg for adults, 150–200 μg of iodine daily for pregnant and lactation women, and 120 μg per day for children aged 6–12 years [4]. Therefore, it is urgent to develop simple, convenient, selective and sensitive sensors for the determination of iodide, especially for food monitoring and disease prevention. Curcumin, 7-bis-(4-hydroxy-3-methoxyphenyl)-1, 6-heptadiene-2,5-dione, is a yellow-orange polyphenol compound derived from the rhizome of *Curcuma longa L.*, which has been commonly used as a spice and natural coloring agent for a long time [5] and a natural additive for food and cosmetics recognized by the WHO and Food and Drug Adminstration (FDA). Also, curcumin has been successfully exploited as a traditional medicine in China and India due to its diverse biological and pharmacological activities, such as lowering blood lipids [6], anti-tumor [7], anti-inflammatory [8], antioxidant [9], anti-hepatotoxicity [10], and anti-bacterial properties [11], which has aroused widespread attention by scholars because of the application of

* Corresponding author.
** Corresponding author.
*** Corresponding author.
E-mail addresses: seesea0304@163.com (H. Yu), huzhizhi@163.com (Z. Hu), weichen@uta.edu (W. Chen).

https://doi.org/10.1016/j.bioactmat.2020.11.006
Received 4 October 2020; Received in revised form 5 November 2020; Accepted 5 November 2020

curcumin in pharmacology and clinical medicine. However, it has been reported that excess curcumin will cause DNA inactivation, lead to a decrease in intracellular ATP levels, and trigger the tissue necrosis [12]. Therefore, quantitative detection of curcumin is of great significance in the fields of food and life sciences.

At present, various detection techniques have been successfully developed to determinate iodide ions and curcumin, such as chromatography [13,14], capillary electrophoresis [15,16], electrochemistry [17,18], and so on. Although these methods possess high accuracy and satisfactory sensitivity, they still display some disadvantages, such as sophisticated instrumentation, complicated sample pretreatment, tedious operation procedures, and unstable electrodes, which are limited to some extent to apply extensively. Thus, none of these methods are suitable for rapid monitoring of the concentration of iodide ions and curcumin. To make up for the above shortcomings, the fluorescence analysis technology represented by carbon dots is extensively favored by researchers due to its low cost, simple operation, fast response, remarkable selectivity, and extraordinary sensitivity [19,20]. As a novel type of zero-dimensional carbon nanomaterial, carbon dots (CDs) not only present tunable optical properties but also exhibit outstanding characteristics including photostability, biocompatibility, low toxicity, easy functionalization, and superior water solubility comparing with traditional organic dyes and semiconductor quantum dots [21]. Because of the excellent optical properties, CDs have shown enormous application prospects in photocatalysis, chemical and biological sensing, bioimaging, photodynamic therapy, and drug delivery [19–24]. Nitrogen-doping is one of the most effective strategies to improve the luminescence properties of CDs. The defects introduced by the nitrogen element induce an upward movement in the Fermi level, increasing the electron activity in the conduction band, which make it possible to efficiently enhance the photoluminescence properties of the CDs [21,25–29]. Naturally, nitrogen-doped CDs have attracted more attention and become a new favorite in the field of nano-sensor and environmental monitoring.

So far, some fluorescence sensors based on CDs have been developed for the detection of iodide ions. Chen et al. [30] exploited a quenching spermine-functionalized carbon dots(SC-dots) to detect I^-, based on the electron transfer between SC-dots and I^-. A detection limit of 0.18 μM was obtained, which was relatively high compared with our present work. Liu et al. [31] fabricated a "turn-off-on" fluorescent method for the detection of I^- based on the CDs/Hg^{2+} fluorescent probe using PEI as the surface passivation reagent. Although this method had a relatively low detection limit (0.084 μM), the raw material cost was relatively high, and the CDs needed to be synthesized under high temperatures and pressures. At present, a variety of functionalized carbon dots have been explored to determine curcumin. Wu et al. [32] synthesize P, N, B co-doped carbon quantum dots using a hydrothermal method, which exhibited extraordinary sensitivity to curcumin with the detection limit of 68 nmol L^{-1}. However, 4-amino-phenylboronic acid as the Boron dopant is toxic to some extent because it contains a benzene ring, which is not environmentally friendly. Hu et al. [26] designed a facile and green approach to synthesize nitrogen and chlorine co-doped CDs for detection curcumin with a low detection limit of 38 nM via the acid-base neutralization heat. However, concentrated hydrochloric acid (HCl) was used as the chlorine dopant in the process of synthesizing CDs. Concentrated HCl is strongly volatile and corrosive, which may irreversibly damage the respiratory organs, eyes, skin and gastrointestinal, *etc*. Thus, exploiting highly sensitive and environmentally friendly CDs with a facile synthetic method without using hazardous reagents is urgently needed. To the best of our knowledge, although numerous fluorescent sensors have been developed to detect either I^- or curcumin, few published reports are available that multi-mechanism detection integrated into one NCDs-based chemosensor was achieved to simultaneously detect both targets.

In the present work, two sensing mechanisms for the detection of I^- and curcumin were integrated into one NCDs-based chemosensor. Firstly, the fluorescence of prepared CDs was quenched due to the specific affinity between the amino/carboxyl groups on the surface of NCDs and Hg^{2+}. With the addition of I^- into the NCDs-Hg^{2+} system, the fluorescence intensity was recovered owing to the extremely strong binding ability between Hg^{2+} and I^-. Consequently, a fluorescence-enhanced sensor was constructed to selectively and sensitively detect I^-, which successfully quantified the trace I^- in water samples and urine sample. Furthermore, since the excitation spectra of NCDs totally overlapped with the ultraviolet absorption spectra of curcumin and a ground-state non-luminescent complex was formed between NCDs and curcumin, which inspired us to established a facile and green N-CDs-based fluorescence quenching sensor for the determination of curcumin based on a synergistic effect of internal filtration effect (IFE) and static quenching. Similarly, the presented fluorescence sensor was satisfactorily used for the quantitation of curcumin in food and environmental water samples. Compared with the previously reported various methods, our proposed fluorescent sensor has shown much remarkable sensitivity, which has a great promising prospect for the detection of I^- and curcumin in biosensing, disease diagnosis, food, and environmental monitoring.

2. Materials and methods

2.1. Reagents

Tartaric acid, urea, curcumin, and quinine sulfate were purchased from Aladdin Chemical Reagent Co., Ltd. (Shanghai, China), and the reagents for metal cation solution, anion solution, drugs, and amino acid solution were purchased from Sinopharm Chemical Reagent Co., Ltd. (Shenyang, China). The experiments were carried out in PBS buffer solution (Na_2HPO_4-NaH_2PO_4, 0.1 M, pH = 7.0). The standard stock solution of Hg^{2+} (0.1 M) is prepared with $Hg(NO_3)_2$. All experimental reagents were of analytical grade and were used directly without further purification. Ultrapure water prepared by the UPTA-30 purification system (18.2 MΩ, Jingwei, China) was used throughout all the experiments.

2.2. Apparatus

The fluorescence spectra were measured by an LS-55 fluorescence spectrophotometer (PerkinElmer, USA). Morphological evaluation and sizes of NCDs were obtained with a JEM-2100 transmission electron microscope (JEOL, Japan) using an accelerating voltage of 200 kV. The X-ray photoelectron spectroscopy (XPS) spectra were recorded on a Thermo ESCALAB 250Xi spectrometer (Thermo Fisher, USA). X-ray diffraction (XRD) measurement was given by X'Pert Powder x-ray diffractometer (PANalytical, Netherlands) with Cu Kα radiation, with voltage and current at 40 kV and 40 mA to show the changes in intersegmental properties. The UV–vis absorption spectra were recorded by a Lambda900 UV–vis spectrophotometer (PerkinElmer, USA). The Fourier transform infrared spectroscopy (FT-IR) spectra were carried out on the Nicolet iS10 FT-IR spectrometer (Thermo Fisher, USA). Chromatographic separations were performed on an ICS 600 ion chromatography (Thermo Fisher Scientific, USA) with a conductivity detector of ASRS-ULTRA suppression mode. The column employed for determination of iodine ion is a Dionex Ionpac AS14 separation column (4 mm × 250 mm) with an Ionpac AG14 guard column (4 mm × 50 mm). Mobile phase consisted of 3.5 mM Na_2CO_3 and 1.0 mM $NaHCO_3$. Flow rate of mobile phase is 1.0 mL min^{-1}. The temperature was controlled at 35 °C. Injection volume is 25 μL. The fluorescence lifetime tests were performed using the FluoroMax-4 TCSPC spectrofluorometer (HORIBA Jobin Yvon, USA). Cyclic voltammogram (CV) curve of NCDs was measured with a CHI 660E electrochemical workstation (Huachen, China) with a platinum wire as counter electrode, and an Ag/AgCl (saturated in 3.0 M of KCl) as reference electrode, and a glassy carbon electrode (diameter 3 mm) modified with NCDs as working electrode.

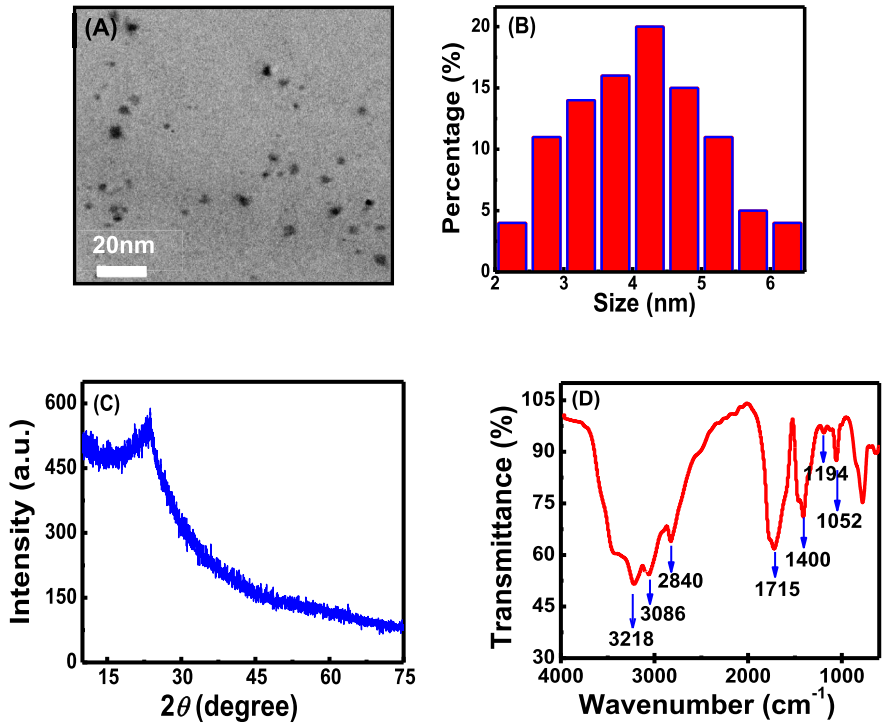

Fig. 1. (A) TEM image, (B) the particle size distribution histogram, (C) XRD spectra and (D) FT-IR spectrum of NCDs.

2.3. Preparation of NCDs

Photoluminescent NCDs were prepared by using tartaric acid as the carbon source and urea as the surface passivation for nitrogen source without any additives by a one-step solid-phase thermal method. Briefly, 0.75 g tartaric acid and 1.20 g urea were placed into an agate mortar. After fully grinding, the mixture was moved into a 30 mL crucible and then was heated in a Muffle furnace at 230 °C for 8 h. During the reaction process, the solid powder undergoes melting, dehydration, polymerization, and carbonization. After being left to cool to room temperature, the fluffy, black, and solid photoluminescent NCDs were obtained. The black product was dissolved in 50 mL deionized water and then centrifuged at 10,000 rpm for 20 min to remove the insoluble and larger particles. Afterwards, the collected supernatant was dialyzed against purified water through a dialysis membrane (MWCO500) for 48 h. Finally, the nitrogen-doped carbon dots powder was obtained after freeze-drying under vacuum conditions at −50 °C for 36 h. And 1.0 mg mL^{-1} carbon dot solution was prepared and stored in a refrigerator at 4 °C for further characterization and application.

2.4. Fluorescence quantum yield (QY) measurement

According to the established method [33], the fluorescence quantum yield (QY) of NCDs was measured with quinine sulfate as the reference (quantum yield is 0.54 in 0.1 M H_2SO_4). The quantum yield of NCDs was calculated according to formula (1):

$$\phi_x = \phi_s \times \left(\frac{Grad_x}{Grad_s}\right) \times \left(\frac{\eta_x}{\eta_s}\right)^2 \quad (1)$$

where subscripts x and s represent NCDs and quinine sulfate, respectively; ϕ is the quantum yield; $Grad$ denotes the slope corresponding to the integrated fluorescence area and absorbance value; η is the refractive index of the solvent. For aqueous solutions, $\eta_x/\eta_s \approx 1$.

2.5. Preparation of NCDs-Hg^{2+} complex

The quenching effect of Hg^{2+} on CDs fluorescence: 18 metal ions related to organism or environment (Na^+, K^+, Ca^{2+}, Mg^{2+}, Ba^{2+}, Cr^{3+}, Hg^{2+}, Co^{2+}, Cd^{2+}, Mn^{2+}, Cu^{2+}, Zn^{2+}, Fe^{3+}, Al^{3+}, Pb^{2+}, La^{3+}, Ni^{2+}, and Ag^+) and 15 anionic ions (HPO_4^{2-}, CO_3^{2-}, HSO_4^-, SO_4^{2-}, PO_4^{3-}, F^-, SO_3^{2-}, CH_3COO^-, HCO_3^-, NO_2^-, HSO_3^-,Br^-, S^{2-}, Cl^-, and I^-) were added into the NCDs solution at the concentration of 100 μM to evaluate the selectivity of the fluorescent sensor. 100 μM of Hg^{2+} and 100 μM of the above-mentioned ions were added into the NCDs solution together to evaluate whether the existence of other ions interfered with the quenching effect of Hg^{2+}.

A working solution was combined by the following: 120 μL of the as-prepared NCDs solution (1.0 mg mL^{-1}), 100 μL of PBS buffer solution (0.1 M, pH 7.0) and different volumes of Hg^{2+} standard solution (0.001 M) were added into a quartz cuvette, followed by the addition of ultrapure water to obtain the total volume of 3.0 mL. After incubating for 1 min at room temperature, the fluorescence spectrum was monitored at the excitation wavelength of 460 nm.

2.6. Detection of I^- by NCDs-Hg^{2+} fluorescence enhanced sensor

Fluorescence recovery effect of I^- on the NCDs-Hg^{2+}system: 120 μL NCDs solution (1 mg mL^{-1}), 100 μL PBS buffer solution (0.1 M, pH 7.0), and 300 μL of Hg^{2+} standard solution (0.001 M) were added into a quartz cuvette. The mixture was vortexed thoroughly for 1 min. Subsequently, different volumes of I^- (0.01 M) was added into this mixture and then diluted to the final volume of 3.0 mL with ultrapure water. The fluorescence recovery of NCDs-Hg^{2+} was recorded. Other competing anions were added to the solution to evaluate the selectivity of the CDs-Hg^{2+} system to I^-.

2.7. Detection of curcumin by NCDs fluorescence quenching sensor

Fourteen kinds of amino acids (Aspartic acid, Lysine, Glutamic acid,

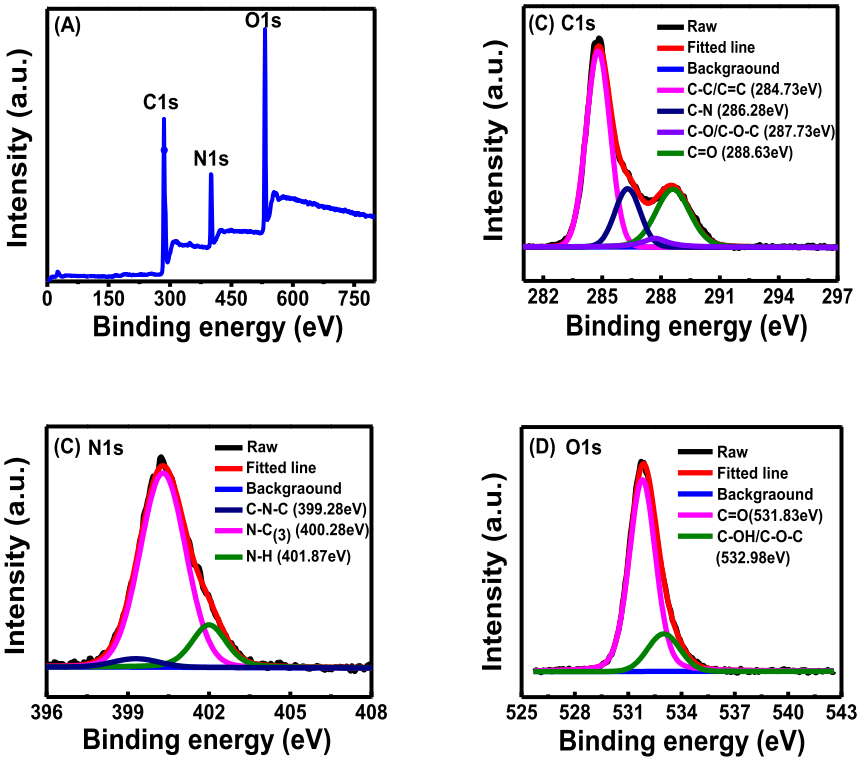

Fig. 2. XPS survey spectrum (A) and high-resolution spectra of C1s (B), N1s (C) and O1s (D) of the NCDs.

Histidine, Arginine, L-tryptophan, L-threonine, Glycine, L-Tyrosine, L-cysteine, L-valine, Leucine, L-methionine, L-serine) and nine kinds of drug molecules (Amoxicillin, Ibuprofen, Rifampin, Roxithromycin, Morin Morin hydrate, Tetracycline Hydrochloride, Levofloxacin, Chloramphenicol, Curcumin) were prepared with the concentration of 0.01 M.

120 μL NCDs solution (1.0 mg mL^{-1}) was added into a quartz cuvette. Then, 100 μL PBS buffer solution (0.1 M, pH 7.0) and 30 μL different types of amino acids or drug molecules (0.01 M) were mixed and diluted with ultra-pure water to the final volume of 3.0 mL. After mixing homogeneously and incubating for 1 min, the fluorescence spectrum was recorded immediately at the excitation wavelength of 460 nm. The slot widths of the excitation and emission were both 10 nm. Other competing substances were added into the NCDs-Cur system to evaluate the selectivity of NCDs. Fluorescence titration was used to investigate the sensitivity of NCDs to curcumin.

2.8. Detection of I^- and curcumin in actual samples

The environmental water samples used in the experiment were taken from the urban area of Anshan, Liaoning Province, and the food samples were taken from the local supermarket, and the urine sample was taken from the healthy people. All the water samples and urine sample were centrifuged at 8000 rpm for 5 min before analysis and then filtered with a 0.22 μm filter membrane for use. Tomato juice was obtained using a plastic juicer. Curry powder, mustard, chili powder, and ginger powder were dissolved in deionized water, respectively, and then transferred to a 10 mL centrifuge tube after ultrasonication and filtration, and centrifuged with a high-speed at 5000 rpm for 10 min. The supernatant was then diluted with deionized water to an appropriate concentration before taking measurements. Then, the standard addition method was used to test the applicability of the sensor.

3. Results and discussion

3.1. Characterization of NCDs

The morphology, particle size, and dispersion of the synthesized NCDs were characterized by transmission electron microscopy (TEM) as shown in Fig. 1A. From the TEM image, we can find that the prepared carbon dots are mostly spherical-shaped and have a uniform dispersion. Fig. 1B is the particle size distribution histogram obtained by statistical analysis of 100 random nanoparticles through Image J software. A narrow size distribution of NCDs ranges from 2.25 nm to 6.25 nm with an average diameter of 4.13 nm ± 0.33 nm, and this may be the origin for the excitation-dependent fluorescence behavior of NCDs. To further explore the microstructure of NCDs, an X-ray diffraction (XRD) test was investigated in Fig. 1C with a broad peak at $2\theta = 23.4°$, which indicated an amorphous carbon phase [20,34,35]. The surface functional groups of NCDs were measured through Fourier transform infrared (FT-IR) spectroscopy (Fig. 1D). Two typical absorption bands appearing at 3218 cm^{-1} and 3086 cm^{-1} are attributed to stretching vibrations of O-H and N-H, respectively. While the absorption peak at 2840 cm^{-1} belongs to the C-H stretching vibration. Also, the characteristic absorption band at 1714 cm^{-1} is corresponds to the C=O stretching vibration. The band appeared at 1400 cm^{-1} indicates the presence of C-N stretching vibration. The peaks at 1194 cm^{-1} and 1052 cm^{-1} are ascribed to the stretching vibrations of C-O-C, and C-OH [36–38]. The above results indicate that nitrogen-doped carbon dots have been successfully prepared with the presence of -OH, -COOH and $-NH_2$ on the surface of NCDs. These functional groups not only improve the hydrophilicity of NCDs and the stability in aqueous solutions but also can interact with some metal ions.

To confirm the conclusions obtained by FT-IR and further examine the functional groups and chemical composition, an X-ray photoelectron spectrometer (XPS) was employed to characterize the synthesized NCDs. Fig. 2A showed the XPS full spectrum of NCDs presented three

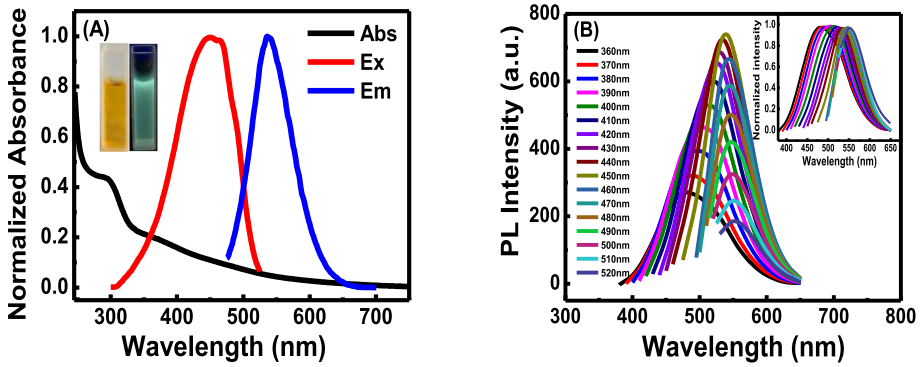

Fig. 3. (A) UV–vis absorption (black line), maximum fluorescence excitation (red line) and maximum emission spectra (blue line) of NCDs in aqueous solution. Inset: photographs of NCDs solution under visible light (left) and 365 nm UV light(right). (B) Fluorescence emission spectra of NCDs under different excitation wavelengths ranging from 360 nm to 520 nm. Inset: normalized fluorescence spectra of NCDs. C_{NCDs} = 0.04 mg mL^{-1}. (For interpretation of the references to color in this figure legend, the reader is referred to the Web version of this article.)

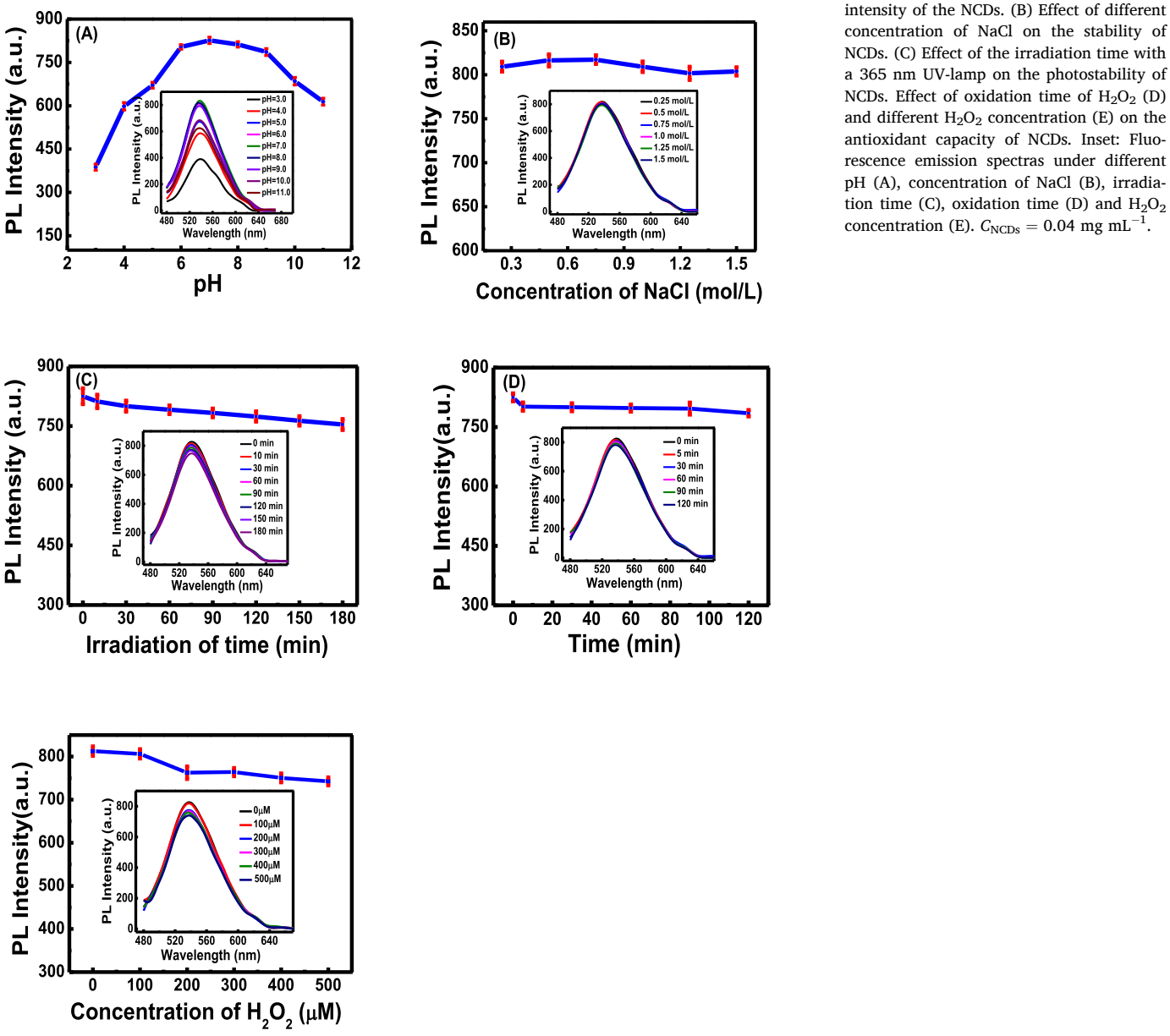

Fig. 4. (A) Effect of pH on the fluorescence intensity of the NCDs. (B) Effect of different concentration of NaCl on the stability of NCDs. (C) Effect of the irradiation time with a 365 nm UV-lamp on the photostability of NCDs. Effect of oxidation time of H_2O_2 (D) and different H_2O_2 concentration (E) on the antioxidant capacity of NCDs. Inset: Fluorescence emission spectras under different pH (A), concentration of NaCl (B), irradiation time (C), oxidation time (D) and H_2O_2 concentration (E). C_{NCDs} = 0.04 mg mL^{-1}.

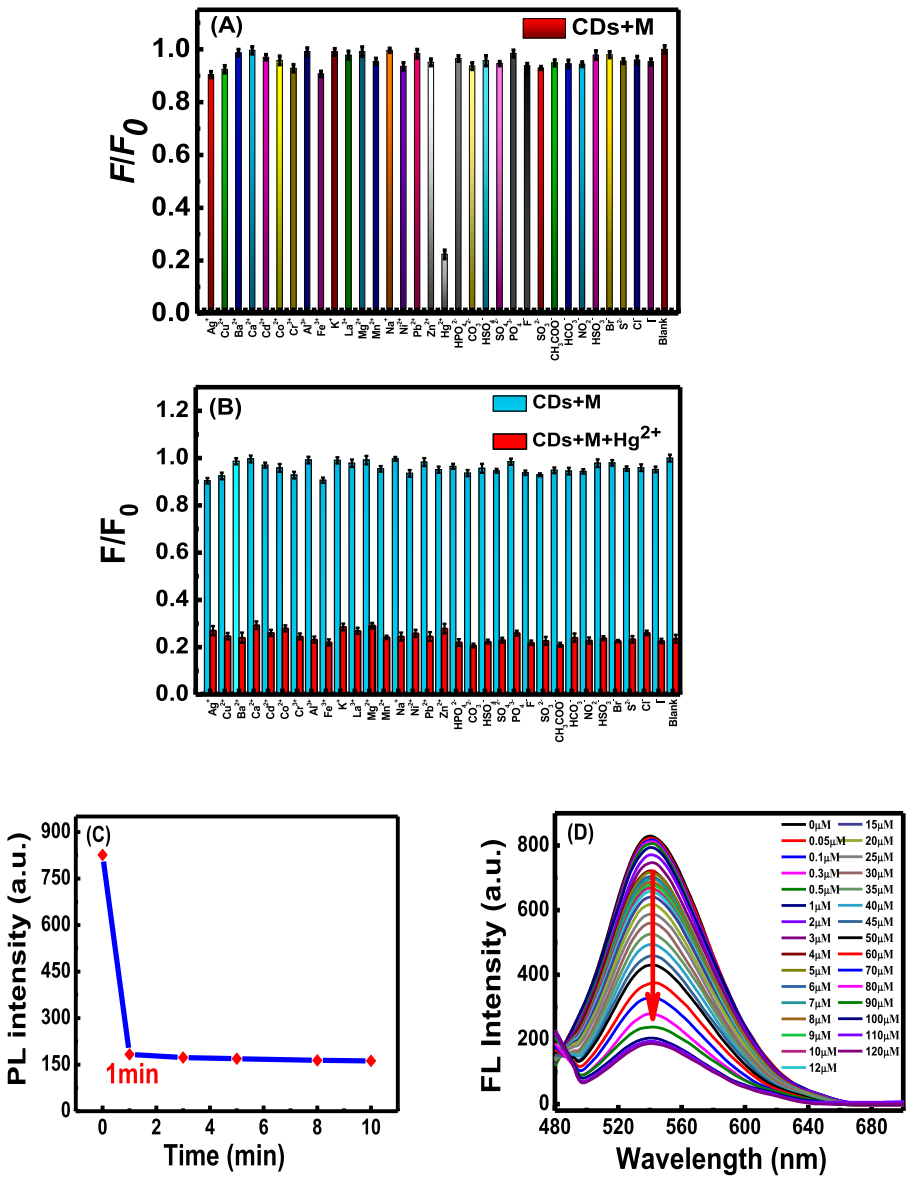

Fig. 5. (A) Fluorescence response (F/F_0) of NCDs (0.04 mg mL^{-1}) in the presence of various mental ions and anion ions at the concentration of 100 μM. (B) Fluorescence response (F/F_0) of NCDs to various ions (100 μM, blue bars) upon addition of 100 μM Hg^{2+} (red bars). (C) The incubation time NCDs with Hg^{2+}. (D) Fluorescence emission spectra of NCDs (0.04 mg mL^{-1}, 0.1 M, pH 7.0 PBS buffer solution) with increasing concentration of Hg^{2+} (from top to bottom: 0–120 μM). (For interpretation of the references to color in this figure legend, the reader is referred to the Web version of this article.)

representative peaks at 285eV, 400eV and 531eV, which corresponded to C1s, N1s and O1s, respectively [35,36]. The Element proportions of NCDs were 57.87% of carbon, 16.22% of nitrogen and 25.91% of oxygen. The high-resolution C1s spectra (Fig. 2B) exhibited four peaks at 284.73, 286.28, 287.73 and 288.63 eV, corresponding to C=C/C-C, C-N, C-O/C-O-C and C=O groups, respectively [29,35,36]. The high-resolution N1s spectra of NCDs (Fig. 2C) depicted three peaks at 399.28, 400.28 and 401.87 eV, which were attributed to C-N-C, N-$(C)_3$ and-N-H groups, respectively [21,26,35,36]. The O1s spectra of NCDs in Fig. 2D presented two peaks at 531.83 and 532.98 eV, which were assigned to C=O and C-OH/C-O-C groups [35,36]. Therefore, all the results indicate that N has been successfully doped to the structure of carbon dots and the NCDs are coated with oxygen-containing functional groups.

3.2. Optical properties of NCDs

The optical properties of the as-synthesized NCDs were investigated by UV–vis and fluorescence spectra. Fig. 3A depicted the UV–vis absorption of NCDs (blank line), an obvious and characteristic absorption peak at 287 nm was observed, which was ascribed to the typical absorption of π-π* transition of C=C [28,32]. There was also a weak absorption band from 300 nm to 400 nm which might be attributed to the n-π* transition of C=O bond [36,37,39,40]. Meanwhile, the maximum emission wavelength (blue line) of NCDs was located at 537 nm with the excitation wavelength (red line) at 460 nm. The NCDs aqueous solution emitted a bright green fluorescence under the irradiation of 365 nm UV light, and it appeared transparent and yellow color in visible light (inset in Fig. 3A). The fluorescence emission spectrum of NCDs was changed with a series of excitation wavelength ranging from 360 nm to 520 nm as shown in Fig. 3B. The maximal fluorescence intensity increased firstly and then decreased. Moreover, the emission wavelength was red-shifted from 470 nm to 560 nm with a maximum emission wavelength at 537 nm (inset in Fig. 3B), which was a typical excitation-dependent fluorescence phenomenon. The fluorescence tunability of as-prepared NCDs is presumably due to the inhomogeneity of the particle sizes and the plenteous emissive traps of surface states formed by the hydroxyl, carboxyl and aminol functional groups [36,37,39,40]. The fluorescence quantum yield of as-fabricated NCDs at room temperature was measured to be 10.5% using quinine sulfate (QY = 54%, 0.1 M H_2SO_4) as reference.

3.3. Fluorescence stability of NCDs

To investigate the fluorescence stability and chemical stability of NCDs aqueous solution, the influences of pH, ionic strength, illumination time, oxidation time, and oxidation concentration on the fluorescence intensity of NCDs were studied. As shown in Fig. 4A, different pH values might have a distinct impact on fluorescence intensity. The NCDs showed the lower fluorescence under the strong acidity or strong alkaline conditions, while exhibited the remarkable fluorescence intensity when pH was neutral (pH = 6.0–9.0). This may be attributed to the abundant carboxyl groups on the surface of NCDs, and hydrogen bonds are easily formed in the strong acidic environment, while H^+ is neutralized in the strong alkaline condition. Due to the destruction of the surface functional groups, the electronic transition of the luminescent center is destroyed, which causes the quenching fluorescence intensity. Thus, the favorable property in a neutral environment makes NCDs excellent candidates in bio-imaging and other biological fields. Fig. 4B depicted that the fluorescence intensities of NCDs had no significant alteration when the concentration of NaCl changed from 0.25 M to 1.5 M, which indicated the outstanding property of salt stability under high ionic strength solutions. Additionally, the NCDs still exhibited good photostability even after continuous irradiation for 3 h with a UV-lamp (Fig. 4C), which demonstrated the excellent resistance to photobleaching of as-prepared NCDs. To survey the oxidation resistance of NCDs, the fluorescence intensities were measured within 120 min after adding H_2O_2 (100 μM) to the NCDs solution (Fig. 4D). And the oxidation resistance of NCDs was also studied by adding different concentrations of H_2O_2 ranging from 0 to 500 μM (Fig. 4E). The results show the fluorescence intensities only slightly change, which verify that as-fabricated NCDs owning great antioxidant capacity. All the above excellent features clearly reveal that the NCDs as fluorescent probes have great potentialities for the analysis of complex matrixes.

3.4. Construction of fluorescence enhanced sensor for detection of I^-

3.4.1. Preparation and optical properties of fluorescence-enhanced sensors

Based on the outstanding optical merits of NCDs in complex environments and the ample functional groups in the structure of NCDs, we further explored the applications in fluorescence sensors. Numerous metal ions could significantly quench the fluorescence of CDs due to the powerful affinity or fast electron transfer [28–31,36,37,39–43], and the CDs-metal ion complex emitted weak fluorescence, which provided a basis for the construction of fluorescence-enhanced sensor. Thus, we investigated the selectivity of as-prepared NCDs toward 18 metal ions including Na^+, K^+, Ca^{2+}, Mg^{2+}, Ba^{2+}, Cr^{3+}, Hg^{2+}, Co^{2+}, Cd^{2+}, Mn^{2+}, Cu^{2+}, Zn^{2+}, Fe^{3+}, Al^{3+}, Pb^{2+}, La^{3+}, Ni^{2+}, and Ag^+ and 15 anionic ions including HPO_4^{2-}, CO_3^{2-}, HSO_4, SO_4^{2-}, PO_4^{3-}, F^-, SO_3^{2-}, CH_3COO^-, HCO_3^-, NO_2^-,HSO_3^- ,Br^-, S^{2-}, Cl^- and I^- at the final concentration of 100 μM. As shown in Fig. 5A, only Hg^{2+} effectively caused fluorescence quenching while the effect of other ions on the fluorescence intensity was almost negligible compared to Hg^{2+}. Fig. 5B described the results of the interference test. The blue bars depicted the fluorescence response (F/F_0) of NCDs to various ions. Subsequently, by adding 100 μM of Hg^{2+}, the fluorescence intensity was noticeably decreased (red bars). It was evident that there was no obvious change in the coexistence of Hg^{2+} and other ions compared with Hg^{2+} alone. The results of selectivity and interference tests demonstrate that NCDs fluorescent probe are able to accurately identify Hg^{2+} in the complex conditions. A possible reason for the excellent selectivity of Hg^{2+} is the mercury ion owns large ion radius and electronic layer structure. Hg^{2+} is easily deformed and polarized to generate non-luminous complexes when it combines with surface functional groups, such as -NH_2, -COOH, -OH [28,31]. To effectively determine Hg^{2+}, the incubation time of NCDs and Hg^{2+} was selected (Fig. 5C). It took only 1 min to reach the maximum fluorescence quenching (at the Hg^{2+}concentration of 100 μM), which suggested that it had a quick and sensitive response for Hg^{2+}. At the same time, the sensitivity of NCDs to Hg^{2+} was examined by adding several concentrations of Hg^{2+} solution to the NCDs aqueous solution. As detailed in Fig. 5D, with the increase of Hg^{2+} concentration ranging from 0 to 120 μM, the fluorescence intensity at 537 nm emission peak position gradually decreased. A near complete fluorescence quenching occurred at the Hg^{2+} concentration over 100 μM, so we chose 100 μM Hg^{2+} for the subsequent studies.

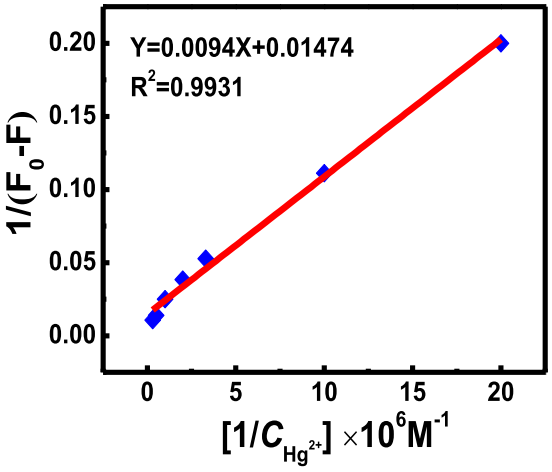

Fig. 6. The relationship between $1/(F_0\text{-}F)$ and $1/C_{Hg}^{2+}$.

Due to the quenching effect of Hg^{2+} on NCDs, the NCDs-Hg^{2+} complexes emitted weak fluorescence. Applying the Lineweaver-Burk double reciprocal equation, the association constant of the NCDs-Hg^{2+} complex could be calculated according to the following equation [44]:

$$\frac{1}{F_0 - F} = \frac{1}{F_0} + \frac{1}{K_{LB} F_0 [Q]} \quad (2)$$

where K_{LB} represents the association constant of NCDs and Hg^{2+}; F_0 and F correspond to the fluorescence intensity of NCDs at the emission of 537 nm in the absence and presence of Hg^{2+}, respectively; [Q] denotes the concentration of quencher (Hg^{2+}). As shown in Fig. 6, calculating the ratio of intercept to slope in the linear equation, the association constant of the NCDs-Hg^{2+} complex was calculated to be 1.6×10^6 L mol^{-1}. Therefore, it is inferred that NCDs can form a stable and strong complex with Hg^{2+}, which makes it possible to fabricate a fluorescence-enhanced sensor for the quantitative determination of I^- in subsequent experiments.

3.4.2. NCDs-Hg^{2+} fluorescence enhanced sensor for detecting I^-

Based on the competitive binding mechanism, the fluorescence recovery properties of the assembled NCDs-Hg^{2+} sensor ($C_{NCDs} = 0.04$ mg mL^{-1} and $C_{[Hg2+]} = 100$ μM) was studied with the addition of various biological relevant anions (Fig. 7A). According to previous reports [45], the solubility product constant of mercury iodide HgI_2 is 2.8×10^{-29}, which is stronger than the association constant of 1.6×10^6 between Hg^{2+} and NCDs. When I^- was added to the NCDs-Hg^{2+} system, Hg^{2+} was completely released from the surface NCDs-Hg^{2+} complex due to the extremely strong affinity between Hg^{2+} and I^-, and the absorption band and surface functional groups of the NCDs were returned to the initial state, and the fluorescence intensity of NCDs-Hg^{2+} was recovered immediately [46]. It had been confirmed that I^- did not exhibit any obvious effects on the fluorescence intensity of NCDs without adding Hg^{2+}, which indicated the recovery of the fluorescence intensity due to the formation of a more stable complex between Hg^{2+} and I^-. As described in Fig. 7A, the fluorescence emission intensity was dramatically recovered upon the addition of 100 μM I^- into the NCDs-Hg^{2+}

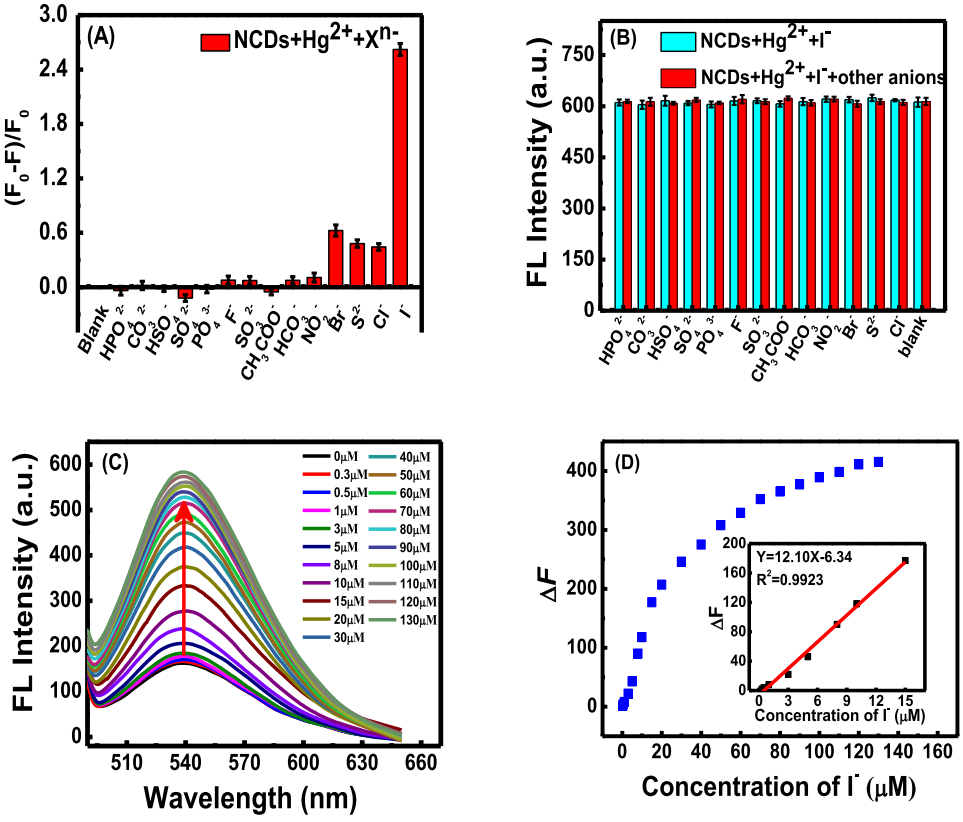

Fig. 7. (A) Fluorescence response $(F_0\text{-}F)/F_0$ of NCDs-Hg^{2+} sensor (C_{NCDs} = 0.04 mg mL^{-1}, C_{Hg}^{2+} = 100 μM) to the various anions (100 μM). (B) Fluorescence intensity of NCDs-Hg^{2+} system with addition of 100 μM of I^- (blue bars) and subsequent addition of various anions (100 μM, red bars). (C) Fluorescence emission spectra of NCDs-Hg^{2+} with increasing concentration of I^-. (D) Plot of the fluorescence intensity of NCDs-Hg^{2+} changing with different I^- concentration (0.3–130 μM). Inset: Linear relationship between ΔF and the concentration of I^- in the range of 0.3–15 μM. (For interpretation of the references to color in this figure legend, the reader is referred to the Web version of this article.)

Table 1
Tolerance of interfering ions for detecting of I^- (C_{NCDs} = 0.04 mg mL^{-1}, C_{Hg}^{2+} = 100 μM, C_{I^-} = 10 μM).

Co-existing ions	Tolerance fold	Co-existing ions	Tolerance fold	Co-existing ions	Tolerance fold
HPO_4^{2-}	50	F^-	100	NO_2^-	50
CO_3^{2-}	75	SO_3^{2-}	100	Br^-	2
HSO_4^-	60	CH_3COO^-	100	S^{2-}	3
SO_4^{2-}	50	HCO_3^-	75	Cl^-	3
PO_4^{2-},	100				

system after 1 min while other anionic ions (100 μM) had no or little effect on the fluorescence recovery. Meanwhile, competition experiments were examined by adding I^- (blue bars) and the mixtures of I^- and other anions (red bars) to the NCDs-Hg^{2+} system (Fig. 7B). It is clearly shown that the influences of other interfering substances on the fluorescence recovering effect are negligible. In addition, competition experiment of I^- was also estimated by increasing the concentration of other potentially interfering ions to examine the tolerance levels with an error of no more than 5%, as shown in Table 1. The results show that the interfering ions are tolerated in relatively high concentration. All the above results demonstrate the NCDs-Hg^{2+} complex can act as a fluorescence-enhanced sensor for the selective determination of I^-.

The sensitivity of NCDs-Hg^{2+} sensor to I^- was evaluated by measuring the fluorescence emission spectra after the addition of various concentrations of I^- (Fig. 7C). The fluorescence intensity at

Table 2
Sensitivity comparison of the proposed sensor with previous methods for I^- detecting.

Detection method	Condition	Linear range (μM)	Detection limit (nM)	Application	Reference
HPLC-DAD	phosphatidylcholine column	3.9–78.8	179	mineral water	[13]
Capillary Electrophoresis	UV detection.	0.20–4.0	60	urine	[15]
Electrochemical	anion-exchange chromatographic separation	–	3900	milk samples, waste waters	[17]
Flow-injection chemiluminescence	$KMnO_4^-$ carbon dots system	3–100	350	food samples	[48]
Fluorescence	spermine-functionalized carbon dots	1–100	180	human serum, HeLa cells	[30]
	CDs-Hg^{2+}	0–70	84	water	[31]
	CDs-Hg^{2+}	0.1–10	72	tap, river, mineral waters, fish	[49]
	DNA-templated gold/silver nanoclusters	0–10	300	spring water, tap water	[50]
	N-CQDs-Hg^{2+}	0–90	92.3	–	[51]
	NCDs-Hg^{2+}	0.3–15	69.4	Tap and mineral waters, urine	This work

Table 3
Determination of I^- in water and human urine samples (n = 3, 95% confidence level).

Real Sample	Initial I^- amount (μM)	Spiked (μM)	Found (μM)	RSD (%)	Recovery (%)
Tap water	0	5.0	5.17 ± 0.28	2.19	103.4
		10.0	9.63 ± 0.32	1.36	96.3
		13.0	12.74 ± 0.49	1.56	98.0
Lake water	0	5.0	4.88 ± 0.27	2.30	97.6
		10.0	9.75 ± 0.34	1.43	97.5
		13.0	13.31 ± 0.46	1.39	102.4
Urine	1.23 ± 0.27 (FL)	5.0	6.47 ± 0.22	1.41	103.8
	1.04 ± 0.32 (IC)	3.0	3.95 ± 0.41	2.03	97.8

around 537 nm was increased gradually with the increase of the concentration of I^-. Fig. 7D depicted the enhanced fluorescence intensity ΔF ($\Delta F = F - F_0$, where F and F_0 represent the emission intensity of the NCDs-Hg^{2+} system at 537 nm in the presence and absence of I^-, respectively) did not fit a linear calibration plot over the whole Hg^{2+} concentration ranging of 0–130 μM. While the inset of Fig. 7D displayed a good linear relationship ($R^2 = 0.9923$) between ΔF and I^- concentration in the range of 0.3–15 μM. The detection limit (LOD) was calculated to be 69.4 nM (8.8 μg L^{-1}) based on equation (3)σ/k. Where σ represents the standard deviation of 11 blank measurements and k is the slope of the linear calibration plot. According to the World Health Organization's urine iodine standard, the content of iodine in urine for healthy people is 100–200 μg L^{-1} (0.78–1.58 μM) [47]. If the consumption of iodine is insufficient or excessive, it will affect thyroid functions and cause thyroid diseases. The LOD of the assembled NCDs-Hg^{2+} fluorescence-enhanced sensor detection of I^- by our method is much lower than the allowed limit, which can be applied to the quantitative determination of I^- in real urine samples. Comparison of analytical methods for detection of I^- reported in the literature (Table 2), the present sensor exhibits superior sensitivity for I^-, such as low detection limit, high sensitivity, good selectivity, low cost of raw material, environmentally friendliness, and excellent water solubility, which can be used to the detection of actual samples.

3.4.3. I^- measurement in real samples

To evaluate the accuracy and feasibility of the fluorescence method, the enhanced sensor NCDs-Hg^{2+} was directly applied for detecting I^- in water and urine samples using a standard addition method. By spiking various concentration of I^- standard solution to the samples, the spike recoveries of this method were calculated. Satisfactory recoveries (96.3%–103.8%) with low relative standard deviation (<5%) were obtained. Meanwhile, in order to verify the accuracy of the proposed fluorescence method, an ion chromatography method was used to detect the initial amount of I^- in the urine sample. The analysis results are displayed in Table 3. It can be seen that there is a good agreement with the results obtained by our proposed fluorescence method, which demonstrates that the proposed NCDs-Hg^{2+} fluorescence-enhanced sensor can be further applied to monitor I^- in the human biological

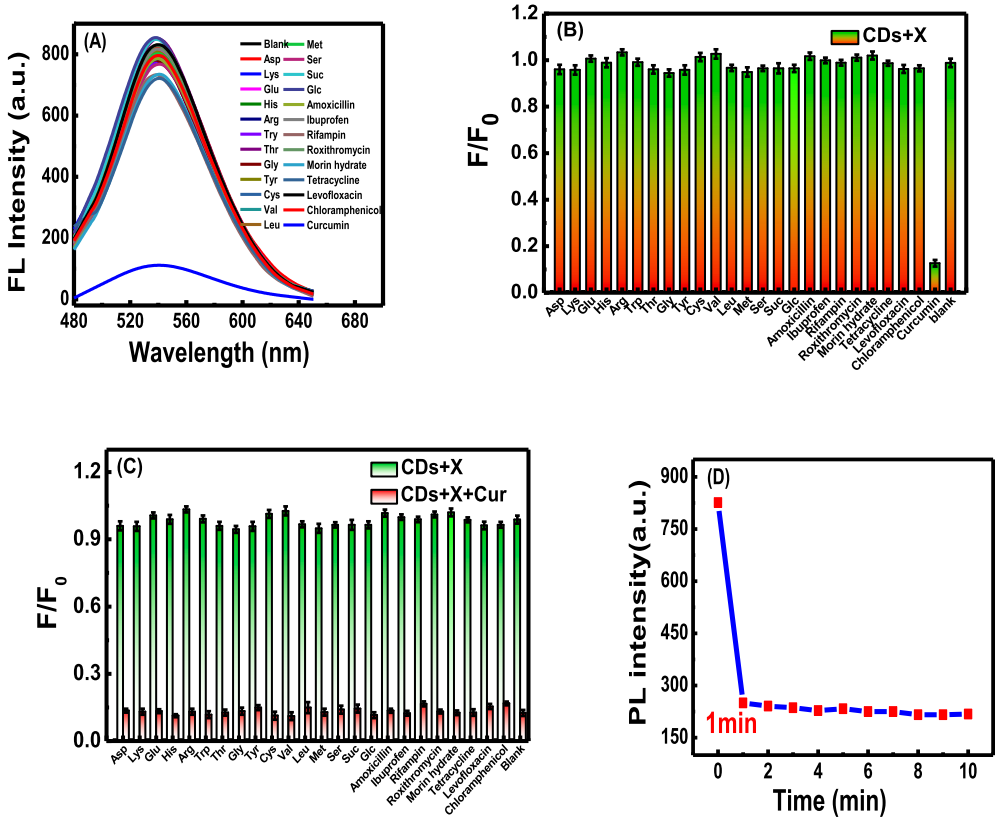

Fig. 8. (A) Fluorescence emission spectra of NCDs to different amino acids and drugs at the concentration of 50 μM. (B) Fluorescence response F/F_0 of NCDs to the various amino acids and drugs. (C) Fluorescence response (F/F_0) of NCDs to various amino acids and other drugs (50 μM, green bars) upon addition of 50 μM curcumin (red bars). (D) Effect of incubation time with curcumin on fluorescence intensity of NCDs. C_{NCDs} = 0.04 mg mL^{-1}. (For interpretation of the references to color in this figure legend, the reader is referred to the Web version of this article.)

Table 4
Tolerance of interfering substances for detecting of curcumin (C_{NCDs} = 0.04 mg mL^{-1}, $C_{curcumin}$ = 10 μM).

Co-existing substances	Tolerance fold	Co-existing substances	Tolerance fold	Co-existing substances	Tolerance fold
Asp	20	Thr	40	Amoxicillin	20
Lys	20	Cys	25	Ibuprofen	20
Glu	15	Val	35	Rifampin	5
His	20	Leu	35	Roxithromycin	10
Arg	20	Met	50	Morin Morin hydrate	5
Trp	30	Ser	50	Tetracycline Hydrochloride	5
Gly	20	Suc	30	Levofloxacin	20
Tyr	35	Glc	50	Chloramphenicol	5

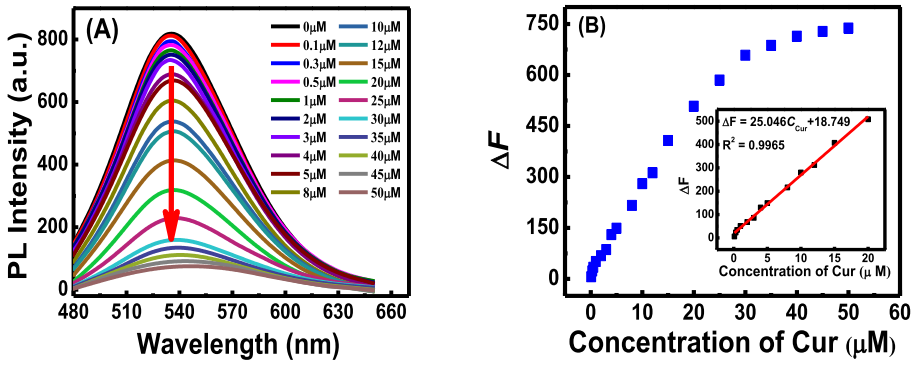

Fig. 9. (A) Fluorescence titration curves of NCDs aqueous solution (0.04 mg mL^{-1}) at different curcumin concentrations (from top to bottom: 0–50 μM). (B) Relationship between ΔF with the full concentration of curcumin ranging from 0 to 50 μM. Inset: Linear relationship between ΔF with the concentration of curcumin (0–20 μM).

samples in real time.

3.5. Quenching fluorescence sensor based on NCDs for detecting curcumin

3.5.1. Fluorescence response of NCDs to curcumin

Due to the existence of abundant surface functional groups and further expanding the possible sensing applications of NCDs, the as-prepared NCDS can be used as a label-free, high-sensitivity quenching fluorescence sensor for the detection of curcumin. At each concentration of 50 μM, the effects of fourteen amino acids (Aspartic acid, Lysine, Glutamic acid, Histidine, Arginine, L-tryptophan, L-threonine, Glycine, L-Tyrosine, L-cysteine, L-valine, Leucine, L-methionine, L-serine) and nine drugs (Amoxicillin, Ibuprofen, Rifampin, Roxithromycin, Morin hydrate, Tetracycline Hydrochloride, Levofloxacin, Chloramphenicol, Curcumin) on the fluorescence performance of NCDs were explored.

Simultaneously, interference tests were conducted with adding 50 μM of curcumin to the above solutions. As shown in Fig. 8A and B, a severe decline was clearly observed by the addition of curcumin, whereas, other amino acids and drugs caused no or slight change on fluorescence response. The effects of coexisting substances on the fluorescence intensity of NCDs quenched by curcumin were almost negligible (Fig. 8C). Table 4 shows the tolerance fold of some interfering species when pre-treating 10 μM curcumin within a ±5% concentration error range. The results indicate that the coexisting amino acids and drugs posed no interference, which reveals that the applicability of NCDs as a precisely selective quenching fluorescence sensor for detection of curcumin. The quenching kinetics results (Fig. 8D) told us that only 1 min of incubation with curcumin was enough to quench the fluorescence NCDs completely.

In addition to the selectivity, the sensitivity of the analytical method plays another important role in evaluating the properties of fluorescence sensing. Fluorescence titration was used to investigate the sensitivity of NCDs' quenching sensor for detecting curcumin. As presented in Fig. 9A, the emission intensity of the NCDs solution around 537 nm declined with the increase of the concentration of curcumin. The fluorescence quenched intensity ΔF ($\Delta F = F_0 - F$, where F_0 and F represent the emission intensity of the NCDs without and with curcumin, respectively) could not fit linearly with the whole curcumin concentration range (0–50 μM) (Fig. 9B), however, there was a good linearity ($\Delta F = 25.046\ C_{Hg}^{2+} + 18.749$, $R^2 = 0.9965$) between ΔF and curcumin concentration ranging from 0.1 to 20 μM. The detection limit (LOD) was estimated to be 29.8 nM based on a signal-to-noise ratio of 3. Compared to the previous reported methods for the determination of curcumin (Table 5), the constructed fluorescence sensor based on NCDs has the advantages of simple preparation procedure, low detection limit, long-wavelength emission, which can be used for a label-free detection of curcumin in actual complex biological samples or food samples.

Table 5
Comparison of different analytical methods for detecting curcumin.

Detection method	Condition	Linear range (μM)	Detection-limit(nM)	Reference
LLME-HPLC	Eurospher C_{18} column	0.217–10869	51.6	[14]
Voltammetry	RGO/CPE	10–6000	3183	[18]
HPLC-PDA	C_{18} column	1.35–54.3	244	[52]
Fluorescence	PNBCDs/λ_{em} = 441 nm	0–1.5	68	[32]
	NCl-CDs/λ_{em} = 467 nm	0.1–35	38	[26]
	N-CDs/λ_{em} = 428 nm	0.78–50	40	[53]
	BN-CDs/λ_{em} = 450 nm	0.2–12.5	65	[25]
	NP-CDs/λ_{em} = 502 nm	0.5–20	58	[27]
	N-CDs/λ_{em} = 537 nm	0.1–20	29.8	This work

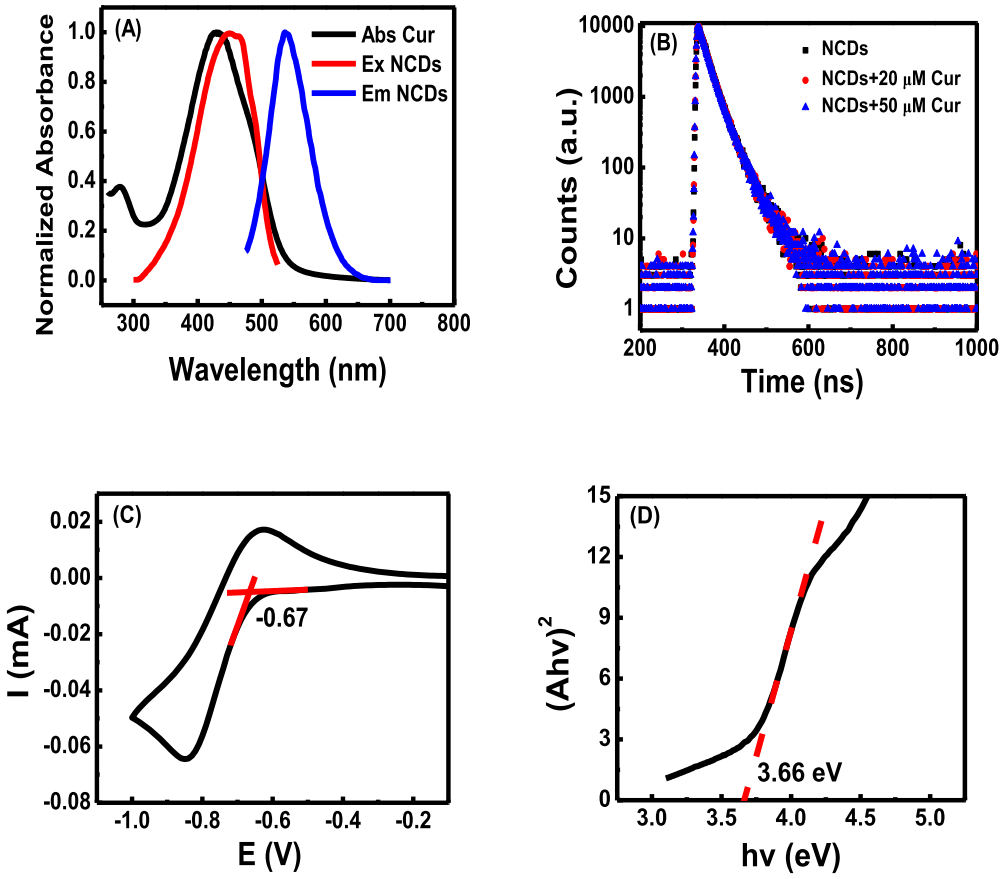

Fig. 10. (A) Overlapping graph of the excitation (red line) and emission spectra (blue line) of NCDs and the UV absorption of curcumin (black line). (B) Fluorescence lifetime of NCDs with various concentrations in the absence and presence of 20 μM and 50 μM curcumin. (C) The cyclic voltammetry curve of NCDs. (D) Band gap calculated from the UV–visible absorption spectrum of NCDs. C_{NCDs} = 0.04 mg mL^{-1}

3.5.2. Possible quenching mechanism for detecting curcumin

To explore the quenching mechanism of NCDs' determination of curcumin, the optical properties of NCDs and curcumin were observed firstly. In general, the quenching mechanism mainly includes fluorescence resonance energy transfer (FRET), photo-induced electron transfer (PET), inner filter effect (IFE), dynamic quenching and static quenching. Among them, FRET, PET, and IFE require a certain degree of overlap between the excitation or emission band of the fluorophore and the absorption band of the quencher, which causes the fluorescence to be quenched [41]. As described in Fig. 10A, the ultraviolet absorption band of curcumin obviously overlapped with the excitation band of NCDs, which was likely to cause the excitation of NCDs to be weakened. Therefore, the possible fluorescence quenching mechanisms may be originating from FRET, PET and IFE. Fig. 10B depicted that the fluorescence decay spectra could be fitted with the bi-exponential curve. The average fluorescence lifetime of NCDs was 25.49 ns. In the presence of 20 μM and 50 μM curcumin, the average fluorescence lifetimes of NCDs were 25.12 ns and 24.99 ns, respectively. Noticeably, the lifetime of NCDs did not change significantly after adding different concentrations of curcumin. This result indicates that the quenching mechanism will not be from dynamic quenching and FRET, which will reduce the fluorescence lifetime of NCDs. To verify whether photo-induced electron transfer quenched the fluorescence of NCDs, the highest occupied orbital (HOMO) and the lowest unoccupied orbital (LUMO) energy levels of NCDs were investigated by using cyclic voltammetry at room temperature. The electrode preparation and detection process were as follows: the concentration of 0.1 mg mL^{-1} NCDs with PBS buffer solution (0.1 M, pH = 7.0) was prepared, then 10 mL of the aforementioned solution was

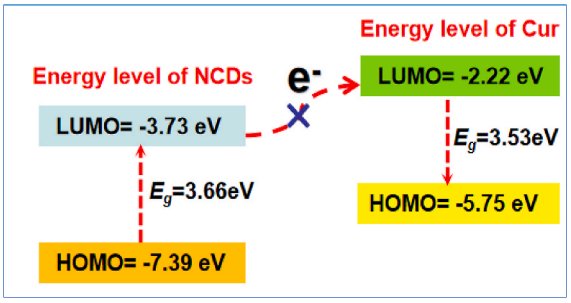

Fig. 11. Electron transfer mechanism of NCDs and curcumin.

dropped onto the surface of a glassy carbon electrode. After leaving it to dry naturally, the prepared working electrode and other two electrodes (Ag/AgCl electrode and the platinum electrode) were put in an electrolytic cell containing PBS buffer solution. Subsequently, the cyclic voltammetry curve was recorded and the reduction potential of NCDs was obtained to be −0.67 eV (Fig. 10C). The E_{HOMO} and E_{LUMO} of NCDs could be calculated by the following empirical formulas [54,55]:

$$E_{LUMO} = -e(E_{red} + 4.4) \quad (3)$$

$$E_{HOMO} = -e(E_{ox} + 4.4) \quad (4)$$

where E_{ox} and E_{red} respectively represent the oxidation and reduction potential of NCDs, respectively. The E_{LUMO} of NCDs was calculated to be

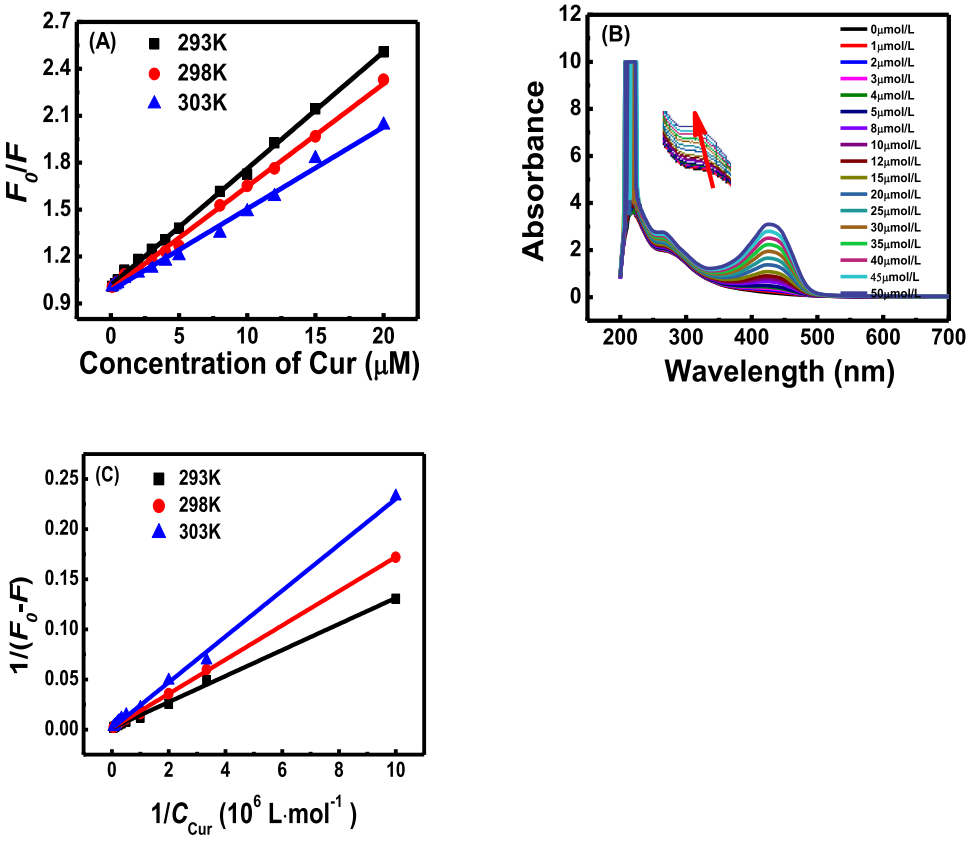

Fig. 12. (A) Stern-Volmer fitting plots of F_0/F versus various concentrations of curcumin at different temperatures. (B) Effect of different concentrations of curcumin on the UV absorption spectrum of NCDs (C_{NCDs} = 0.04 mg mL^{-1}). Inset: the enlarged image of the absorption peak at 287 nm. (C) Lineweaver-Burk plots of $1/(F_0\text{-}F)$ versus $1/C_{Cur}$ at different temperatures.

Table 6
K_{SV}, K, linear equation and correlation coefficient of Stern-Volmer and Lineweaver-Burk equations.

	Stern-Volmer			Lineweaver-Burk		
T(K)	K_{SV} (10^4L·mol^{-1})	Linear fitting equation	R^2	K_{LB} (10^4L·mol^{-1})	Linear fitting equation	R^2
293	7.46	F_0/F = 0.0747[Cur]+1.0145	0.9989	11.3	$(F_0\text{-}F)^{-1}$ = 0.0129[Cur]$^{-1}$+0.0015	0.9977
298	6.57	F_0/F = 0.0657[Cur]+0.9906	0.9971	9.31	$(F_0\text{-}F)^{-1}$ = 0.0171[Cur]$^{-1}$+0.0016	0.9995
303	5.23	F_0/F = 0.0524[Cur]+0.9810	0.9907	6.03	$(F_0\text{-}F)^{-1}$ = 0.0229[Cur]$^{-1}$+0.0014	0.9978

−3.73 eV according to formula (3). Due to the irreversibility of the oxidation process, the E_{HOMO} could not be obtained by formula (4). Analyzing the band gap (E_g) in combination with the ultraviolet absorption spectrum of NCDs (Fig. 10D), and E_g was calculated to be 3.66 eV. Then, the E_{HOMO} of NCDs could be obtained by formula (5) [56]:

$$E_{HOMO} = E_{LUMO} - E_g \quad (5)$$

So, the E_{HOMO} of NCDs was estimated to be −7.39 eV. The E_{HOMO} and E_{LUMO} of curcumin were −5.75 eV and −2.22 eV respectively according to the literature [32]. It can be seen from Fig. 11 that the excited state electrons of NCDs can not be transferred from the LUMO of NCDs to the LUMO of curcumin, so the fluorescence quenching of NCDs is not caused by photo-induced electron transfer. In summary, the quenching mechanism of NCDs for the detection of curcumin is likely to be dominated by the internal filtration effect (IFE).

Fig. 10B demonstrated that the fluorescence lifetime of NCDs was not quenched by curcumin, speculating that the quenching process may be caused by static quenching. To further confirm the static quenching mechanism, the standard Stern-Volmer equation $\frac{F_0}{F} = 1 + K_{sv}[Q]$ was applied to judge the quenching type [28,57]. Where K_{sv} represents the quenching constant of NCDs. F and F_0 represent the emission intensity of the NCDs at 537 nm in the presence and absence of curcumin, respectively. [Q] is the concentration of curcumin. The Stern-Volmer plots of F_0/F versus the various concentrations of curcumin at three different temperatures illustrated a good linear correlation (Fig. 12A), and the quenching constant (K_{sv}) declined from 7.47 × 10^4 L mol^{-1} to 5.23 × 10^4 L mol^{-1} with the increase of temperature (Table 6), affirming that the quenching process was a static quenching mechanism.

In the static quenching process, a non-fluorescent or weak fluorescent complex is formed between the quencher and the ground state fluorescent molecule, which changes the ultraviolet absorption spectrum of the fluorescent substance. As presented in Fig. 12B, the UV absorption intensity gradually strengthened with the increases of concentration of curcumin. Meanwhile, the absorption peak at 287 nm gradually shifted to about 270 nm. It is speculated that the surface functional groups of NCDs and curcumin form a ground-state complex, which causes the change of absorption spectrum of NCDs. The static quenching association constant can be obtained by the Lineweaver-Burk double reciprocal equation (2). From Table 6, we can see that the association constant K_{LB} of the NCDs-curcumin complex shows a

Table 7
Applications of NCDs in water samples for the determination of curcumin (n = 3, 95% confidence level).

Real Sample	Initial Cur amount (μM)	Spiked (μM)	Found (μM)	RSD (%)	Recovery (%)
Running water	0	5.0	5.08 ± 0.15	1.23	101.6
		10.0	10.36 ± 0.22	0.86	103.6
		15.0	14.58 ± 0.57	1.60	97.2
Mineral water	0	5.0	4.92 ± 0.23	1.86	98.4
		10.0	10.05 ± 0.26	1.05	100.5
		15.0	14.35 ± 0.42	1.19	95.7
Lake water	0	5.0	5.13 ± 0.28	2.21	102.6
		10.0	10.15 ± 0.24	0.94	101.5
		15.0	15.73 ± 0.61	1.56	104.8

Table 8
Applications of NCDs in food samples for the determination of curcumin (n = 3, 95% confidence level).

Real Sample	Initial Cur amount (μM)	Spiked (μM)	Found (μM)	RSD (%)	Recovery (%)
Cayenne pepper	2.31	5.0	7.59 ± 0.27	1.47	103.8
Ginger pepper	1.74	5.0	6.59 ± 0.35	2.14	97.7
Curry powder	1.12	5.0	6.11 ± 0.21	1.42	99.8
Tomato juice	2.41	5.0	7.57 ± 0.39	2.08	102.1
Mustard	2.17	5.0	7.40 ± 0.19	1.02	103.2

downward trend with the rise of temperature, indicating that the ground-state complex gradually decomposes and the stability of the complex decreases. These results again demonstrate the fluorescence quenching is caused by static quenching. In conclusion, the quenching mechanism of present NCDS on curcumin results from the synergistic effect of internal filtration effect and static quenching.

3.5.3. Application of NCDs in water and food samples

Currently, curcumin is one of the large-scale applications of natural edible colorings, which is also a widely used non-steroidal anti-inflammatory and anti-cancer drug. So, it is necessary to evaluate the feasibility of NCDs' quenching fluorescent sensor for the detection of curcumin in actual samples. The standard addition tests were used to estimate the accuracy and reproducibility of the present analysis method (Tables 7 and 8). Curcumin was not detected in water samples (tap water, mineral water and lake water). By adding 5 μM, 10 μM and 15 μM curcumin respectively, the spiked recoveries in water samples were measured to be between 95.7% and 104.8% with RSD between 0.86% and 2.21%. At the same time, curcumin was detected in foods (curry powder, mustard, chili powder, ginger powder and tomato juice) by the same fluorescent sensors. After adding 5 μM curcumin, the recoveries of standard addition were between 97.7% and 103.8% with a lower RSD. The above results show that the as-fabricated fluorescent quenching sensor for quantitative detection of curcumin is accurate, reliable and reproducible, which is promising to monitor curcumin in real samples.

4. Conclusion

In summary, a facile, fast, cheap and environmental-friendly route to construct nitrogen-doped carbon dots (NCDs) with green emission was developed using a one-step solvent-free solid phase method with inexpensive tartaric acid and urea as precursors. The as-synthesized NCDs possessed an amorphous carbon structure with a narrow size distribution. The surface of NCDs was covered with numerous functional groups, such as hydroxyl, carboxyl and amino groups, which made it possible to react with various targets. An NCDs-based fluorescence-enhanced sensor was explored for sensitive detection I^- in the presence of Hg^{2+} due to the formation of HgI_2 complex with a detection limit of 69.4 nM, which has been applied to detect I^- in water and urine samples. Based on a mutual effect of internal filtration effect (IFE) and static quenching, fluorescence intensity was quenched gradually with the addition of curcumin. Moreover, a lower detection limit of 29.8 nM and satisfactory recoveries with 95.7–104.8% were achieved to determine curcumin in food and environmental water samples. According to the above results, our fluorescence enhanced/quenching sensor has an extremely high potential for practical applications in the detection and monitoring of iodine and curcumin detection in water, biological and food samples.

CRediT authorship contribution statement

Xiaodan Tang: Methodology. **Hongmei Yu:** Conceptualization, Writing - original draft. **Brian Bui:** Formal analysis, Writing - review & editing. **Lingyun Wang:** Writing - original draft. **Christina Xing:** Formal analysis, Writing - review & editing. **Shaoyan Wang:** Funding acquisition. **Mingli Chen:** Writing - original draft. **Zhizhi Hu:** Funding acquisition. **Wei Chen:** Conceptualization, Writing - original draft.

Declaration of competing interest

The authors declare that they have no known competing financial interests or personal relationships that could have appeared to influence the work reported in this article.

Acknowledgments

Financial supports from the XingLiao Talent Project Grants (No. XLYC1902076) and the University of Science and Technology Liaoning Talent Project Grants (No. 601010302) are highly appreciated. We gratefully acknowledge the support from Ningbo Cuiying Chemical Technology Co., LTD. WC would like to thank the distinguished award from UA Arlington.

References

[1] M.B. Zimmermann, K. Boelaert, Iodine deficiency and thyroid disorders, Lancet Diabet. Endo 3 (2015) 286–295.
[2] J.W. Liu, L.X. Liu, Q.Z. Jia, X.D. Zhang, X. Jin, H.M. Shen, Effects of excessive iodine intake on blood glucose, blood pressure, and blood lipids in adults, Biol. Trace Elem. Res. 192 (2019) 136–144.
[3] F. Azizi, M. Hedayati, M. Rahmani, R. Sheikholeslam, S. Allahverdian, N. Salarkia, Reappraisal of the risk of iodine-induced hyperthyroidism: an epidemiological population survey, J. Endocrinol. Invest. 28 (2005) 23–29.
[4] A. Moreda-Pijñeiro, V. Romarís-Hortas, P. Bermejo-Barrera, A review on iodine speciation for environmental, biological and nutrition fields, J. Anal. At. Spectrom. 26 (2011) 2107–2152.
[5] F.Y. Ye, D.D. Lei, S.M. Wang, G.H. Zhao, Polymeric micelles of octenylsuccinated corn dextrin as vehicles to solubilize curcumin, Food Sci. Technol. 75 (2017) 87–194.
[6] S. Sarker, M. Haque, K. Sujan, M. Talukder, M. Miah, Curcumin attenuates butter fat induced hyperlipidemia in mice, J. Bangladesh Agric. Univ. 17 (2019) 220–225.
[7] I.R. Suhito, W. Lee, S. Baek, D. Lee, J. Min, Rapid and sensitive electrochemical detection of anticancer effects of curcumin on human glioblastoma cells, Sensor. Actuator. B Chem. 288 (2019) 527–534.
[8] C. Porro, A. Cianciulli, T. Trotta, D.D. Lofrumento, M.A. Panaro, Curcumin regulates anti-inflammatory responses by JAK/STAT/SOCS signaling pathway in BV-2 microglial cells, Biology 8 (2019) 51–63.

[9] Z. Hussain, H.E. Thu, M.W. Amjad, F. Hussain, T.A. Ahmed, S. Khan, Exploring recent developments to improve antioxidant, anti-inflammatory and antimicrobial efficacy of curcumin: a review of new trends and future perspectives, Mater. Sci. Eng. C 77 (2017) 1316–1326.

[10] S.S.D. Kumar, N.N. Houreld, H. Abrahamse, Therapeutic potential and recent advances of curcumin in the treatment of aging-associated diseases, Molecules 23 (2018) 835–849.

[11] G. Marslin, J. Prakash, S. Qi, G. Franklin, Oral delivery of curcumin polymeric nanoparticles ameliorates CCl_4-induced subacute hepatotoxicity in wistar rats, Polymers 10 (2018) 541–553.

[12] H. Mirzaei, A. Shakeri, B. Rashidi, A. Jalili, Z. Banikazemi, A. Sahebkar, Phytosomal curcumin: a review of pharmacokinetic, experimental and clinical studies, Biomed. Pharmacother. 85 (2017) 102–112.

[13] M. Tatarczak-Michalewska, J. Flieger, J. Kawka, W. Flieger, E. Blicharska, HPLC-DAD determination of iodide in mineral waters on phosphatidylcholine column, Molecules 24 (2019) 1243–1257.

[14] N. Khorshidi, M. Rahimi, I. Salimikia, Application of aeration-assisted homogeneous liquid-liquid microextraction procedure using Box-Behnken design for determination of curcumin by HPLC, J. Separ. Sci. 43 (2020) 2513–2520.

[15] A.N.d. Macedo, K. Teo, A. Mente, M.J. McQueen, J. Zeidler, P. Poirier, S.A. Lear, A. Wielgosz, P. Britz-McKibbin, A robust method for iodine status determination in epidemiological studies by capillary electrophoresis, Anal. Chem. 86 (2014) 10010–10015.

[16] S. Anubala, R. Sekar, K. Nagaiah, Development and validation of an analytical method for the separation and determination of major bioactive curcuminoids in Curcuma longarhizomes and herbal products using non-aqueous capillary electrophoresis, Talanta 123 (2014) 10–17.

[17] T.R.I. Cataldi, A. Rubino, R. Ciriello, Sensitive quantification of iodide by ion-exchange chromatography with electrochemical detection at a modified platinum electrode, Anal. Bioanal. Chem. 382 (2005) 134–141.

[18] M. Rahimnejad, R. Zokhtareh, A.A. Moghadamnia, M. Asghary, An electrochemical sensor based on reduced graphene oxide modified carbon paste electrode for curcumin determination in human blood serum, Port. Electrochim. Acta 38 (2020) 29–42.

[19] K.K. Chan, S.H.K. Yap, K.T. Yong, Biogreen synthesis of carbon dots for biotechnology and nanomedicine applications, Nano-Micro Lett. 10 (2018) 72.

[20] Y. Wang, Y. Zhu, S. Yu, C. Jiang, Fluorescent carbon dots: rational synthesis, tunable optical properties and analytical applications, RSC Adv. 7 (2017) 40973–40989.

[21] F. Yan, Z. Sun, H. Zhang, X. Sun, Y. Jiang, Z. Bai, The fluorescence mechanism of carbon dots, and methods for tuning their emission color: a review, Microchim. Acta 186 (2019) 583.

[22] S. Chen, T. Sun, M. Zheng, Z. Xie, Carbon dots based nanoscale covalent organic frameworks for photodynamic therapy, Adv. Funct. Mater. 30 (2020), 2004680.

[23] S.Y. Lu, L.Z. Sui, J.J. Liu, S.J. Zhu, A.M. Chen, M.X. Jin, B. Yang, Near-Infrared photoluminescent polymer-carbon nanodots with two-photon fluorescence, Adv. Mater. 29 (2017), 1603443.

[24] H.Q. Song, X.J. Liu, B.Y. Wang, Z.Y. Tang, S.Y. Lu, High production-yield solid-state carbon dots with tunable photoluminescence for white/multi-color light-emitting diodes, Sci. Bull. 64 (2019) 1788–1794.

[25] W. Bian, X. Wang, Y.K. Wang, H.F. Yang, J.L. Huang, Z.W. Cai, M.M.F. Choi, Boron and nitrogen co-doped carbon dots as a sensitive fluorescent probe for the detection of curcumin, Luminescence 33 (2018) 174–180.

[26] Q. Hu, L. Gao, S.Q. Rao, Z.Q. Yang, T. Li, X.J. Gong, Nitrogen and chlorine dual-doped carbon nanodots for determination of curcumin in food matrix via inner filter effect, Food Chem. 280 (2019) 195–202.

[27] Y. Liu, X.J. Gong, W.J. Dong, R.X. Zhou, S.M. Shuang, C. Dong, Nitrogen and phosphorus dual-doped carbon dots as a label-free sensor for curcumin determination in real sample and cellular imaging, Talanta 183 (2018) 61–69.

[28] H. Wu, C. Tong, Nitrogen- and sulfur-codoped carbon dots for highly selective and sensitive fluorescent detection of Hg^{2+} ions and sulfide in environmental water samples, J. Agric. Food Chem. 67 (2019) 2794–2800.

[29] Z. Han, H. Zhang, L. He, S. Pan, H. Liu, X.L. Hu, One-pot hydrothermal synthesis of nitrogen and sulfur co-doped carbon dots and their application for sensitive detection of curcumin and temperature, Microchem. J. 146 (2019) 300–308.

[30] J.Q. Chen, X.W. Liu, X.L. Hou, Y.Y. Chen, F.F. Xing, L.Y. Feng, Label-free iodide detection using functionalized carbon nanodots as fluorescent probes, Anal. Bioanal. Chem. 412 (2020) 2893–2901.

[31] X.Q. Liu, X. Wei, Y.Q. Xu, H.J. Li, K. Lu, K. Wang, Y.S. Yan, A novel fluorescent nanoswitch based on carbon dots for sensitive detection of Hg^{2+} and I, Nano 12 (2017), 1750024.

[32] B. Wu, X.L. Liu, X.F. Shi, W. Han, C.R. Wang, L. Jiang, Highly photoluminescent and temperature sensitive P, N, B-co-doped carbon quantum dots and their highly sensitive recognition for curcumin, RSC Adv. 9 (2019) 8340–8349.

[33] V. Borse, M. Thakur, S. Sengupta, R. Srivastava, N-doped multi-fluorescent carbon dots for "turn off-on" silver-biothiol dual sensing and mammalian cell imaging application, Sensor. Actuator. B Chem. 248 (2017) 481–492.

[34] X. Wen, P. Yu, Y.-R. Toh, X. Hao, J. Tang, Intrinsic and extrinsic fluorescence in carbon nanodots: ultrafast time-resolved fluorescence and carrier dynamics, Adv. Opt. Mater. 1 (2013) 173–178.

[35] P.K. Chu, L. Li, Characterization of amorphous and nanocrystalline carbon films, Mater. Chem. Phys. 96 (2006) 253–277.

[36] H. Ding, S.B. Yu, J.S. Wei, H.M. Xiong, Full-color light-emitting carbon dots with a surface-state-controlled luminescence mechanism, ACS Nano 10 (1) (2016) 484–491.

[37] H. Zheng, Q. Wang, Y. Long, H. Zhang, X. Huang, R. Zhu, Enhancing the luminescence of carbon dots with a reduction pathway, Chem. Commun. 47 (2011) 10650–10652.

[38] S. Zhu, L. Wang, B. Li, Y. Song, X. Zhao, G. Zhang, S. Zhang, S. Lu, J. Zhang, H. Wang, H. Sun, B. Yang, Investigation of photoluminescence mechanism of graphene quantum dots and evaluation of their assembly into polymer dots, Carbon 77 (2014) 462–472.

[39] Z. Sun, X. Li, Y. Wu, C. Wei, H. Zeng, Origin of green luminescence in carbon quantum dots: specific emission bands originate from oxidized carbon groups, New J. Chem. 42 (2018) 4603–4611.

[40] P. Zhu, K. Tan, Q. Chen, J. Xiong, L. Gao, Origins of efficient multiemission luminescence in carbon dots, Chem. Mater. 31 (2019) 4732–4742.

[41] J. Hou, Z. Tian, H. Xie, Q. Tian, S. Ai, A fluorescence resonance energy transfer sensor based on quaternized carbon dots and Ellman's test for ultrasensitive detection of dichlorvos, Sensor. Actuator. B Chem. 232 (2016) 477–483.

[42] X. Jiang, J. Huang, T. Chen, Q. Zhao, F. Xu, X. Zhang, Synthesis of hemicellulose/deep eutectic solvent based carbon quantum dots for ultrasensitive detection of Ag^{+} and L-cysteine with "off-on" pattern, Int. J. Biol. Macromol. 153 (2020) 412–420.

[43] Z. Li, H.J. Yu, T. Bian, Y.F. Zhao, C. Zhou, L. Shang, Y.H. Liu, L.Z. Wu, C.H. Tung, T. R. Zhang, Highly luminescent nitrogen-doped carbon quantum dots as effective fluorescent probes for mercuric and iodide ions, J. Mater. Chem. C 3 (2015) 1922–1928.

[44] H.X. Zhang, X. Huang, P. Mei, K.H. Li, C.N. Yan, Studies on the interaction of tricyclazole with β-cyclodextrin and human serum albumin by spectroscopy, J. Fluoresc. 16 (2006) 287–294.

[45] H.M. Zhang, Y.B. Li, X.L. Liu, P.R. Liu, Y. Wang, T.C. An, H.G. Yang, D.W. Jing, H. J. Zhao, Determination of iodide via direct fluorescence quenching at nitrogen-doped carbon quantum dot fluorophores, Environ. Sci. Technol. Lett. 1 (2014) 87–91.

[46] Y.J. Huang, J.Y. Zhou, C. Lian, Z.C. Huang, X.H. Kang, Z.Y. Huang, X.J. Li, L. Chen, Y. Guan, Investigation of excitation-, pH-, metal ion-, temperature-, and polarity dependent fluorescence of carbon dots derived from silkworm excrement, Acta Phys. Chim. Sin. 35 (2019) 1267–1275.

[47] F.K. Du, F. Zeng, Y.H. Ming, Carbon dots-based fluorescent probes for sensitive and selective detection of iodide, Microchim. Acta 180 (2013) 453–460.

[48] S.Q. Han, B.B. Liu, Z.Y. Fan, L.F. Zhang, F.Y. Jiang, Chemiluminescence detection of trace iodide with flow injection analysis of $KMnO_4$-carbon dots system, Luminescence 32 (2017) 1192–1196.

[49] R. Tabaraki, N. Sadeghinejad, Microwave assisted synthesis of doped carbon dots and their application as green and simple turn off-on fluorescent sensor for mercury (II) and iodide in environmental samples, Ecotoxicol. Environ. Saf. 153 (2018) 101–106.

[50] Z.H. Li, R.Y. Liu, G.F. Xing, T. Wang, S.Y. Liu, A novel fluorometric and colorimetric sensor for iodide determination using DNA-templated gold/silver nanoclusters, Biosens. Bioelectron. 96 (2017) 44–48.

[51] H. Huang, Y.H. Weng, L.H. Zheng, B.X. Yao, W. Weng, X.C. Lin, Nitrogen-doped carbon quantum dots as fluorescent probe for "off-on" detection of mercury ions, L-cysteine and iodide ions, J. Colloid Interface Sci. 506 (2017) 373–378.

[52] E.S. Vieira, E. Lemos-Senn, Application of a new validated HPLC-PDA method for simultaneous determination of curcumin and melatonin in hyaluronic acid-coated nanoemulsions, J. Braz. Chem. Soc. 31 (2020) 467–475.

[53] M.M.F. Baig, Y.C. Chen, Bright carbon dots as fluorescence sensing agents for bacteria and curcumin, J. Colloid Interface Sci. 501 (2017) 341–349.

[54] Y.Z. Fan, Y. Zhang, N. Li, S.G. Liu, T. Liu, N.B. Li, H.Q. Luo, A facile synthesis of water-soluble carbon dots as a label-free fluorescent probe for rapid, selective and sensitive detection of picric acid, Sensor. Actuator. B Chem. 240 (2017) 949–955.

[55] Y.N. Zhao, S.Y. Zou, D.Q. Huo, C.J. Hou, M. Yang, J.J. Li, M.H. Bian, Simple and sensitive fluorescence sensor for methotrexate detection based on the inner filter effect of N, S co-doped carbon quantum dots, Anal. Chim. Acta 1047 (2019) 179–187.

[56] N. Amin, A. Afkhami, L. Hosseinzadeh, T. Madrakian, Green and cost-effective synthesis of carbon dots from date kernel and their application as a novel switchable fluorescence probe for sensitive assay of Zoledronic acid drug in human serum and cellular imaging, Anal. Chim. Acta 1030 (2018) 183–193.

[57] H.F. Wu, J.H. Jiang, X.T. Gu, C.L. Tong, Nitrogen and sulfur co-doped carbon quantum dots for highly selective and sensitive fluorescent detection of Fe(III) ions and L-cysteine, Microchim. Acta 184 (2017) 2291–2298.